Magnetic field effect on the thresholds of a sequence of transitions in the electroconvection of a homeotropic nematic liquid crystal

Nándor Éber,[1] Szilárd Németh,[1] Axel G. Rossberg,[2] Lorenz Kramer,[3] and Ágnes Buka[1]

[1]*Research Institute for Solid State Physics and Optics, Hungarian Academy of Sciences, P.O.B. 49, H-1525 Budapest, Hungary*
[2] *Institut für Datenanalyse und Modellbildung, University of Freiburg, D-79104 Freiburg, Germany*
[3] *Institute of Physics, University of Bayreuth, D-95440 Bayreuth, Germany*

We present a detailed analysis of the characteristics of electroconvection patterns in a homeotropic nematic liquid crystal under the influence of a variable magnetic field. An unambiguous observation of low frequency "reentrant" normal rolls and a nonmonotonic magnetic field dependence of the threshold voltages is reported. The effect of the magnetic field on the normal roll—abnormal roll transition is determined, which is in good agreement with theoretical predictions of the weakly nonlinear analysis.

I. INTRODUCTION

Electroconvection (EC) in a thin ($d \sim 10\text{-}100$ μm) layer of liquid crystals is a well known example of pattern forming instabilities in complex, nonequilibrium systems [1]. It is a threshold phenomenon that is usually observed in a slightly conducting nematic with a positive conductivity and negative dielectric anisotropy. Varying easily tunable control parameters (rms voltage V, frequency f, magnetic field H, etc.) and/or the orientation of the liquid crystal it can provide a wide variety of scenarios.

In planar nematics a preferred direction $(\vec{x})$ exists in the plane of the layer due to an anisotropic surface treatment. In homeotropic cells the director is normal to the surfaces (along $\vec{z}$) and electroconvection is preceded by a *bend Fréedericksz transition*. Ideally, in this geometry the tilt direction of the director and hence its in-plane (xy) component is selected accidentally by a spontaneous symmetry breaking due to the isotropy of the surface treatment, which leads to chaotic patterns already at the onset of electroconvection [soft mode turbulence] [2–8]. This isotropy can be removed, however, by a small magnetic field $\vec{H} \| \vec{x}$ applied parallel to the surfaces [3,7–14], then the electroconvection scenarios resemble (qualitatively) those in the planar case [1].

In an appropriate frequency range ($f_L < f < f_c$) the EC pattern appears at the *electroconvection threshold* voltage V_c as "conductive" normal rolls (NR), oriented perpendicular to the in-plane component of the director. Below the frequency f_L (the Lifshitz point), the rolls are usually tilted in one of two symmetrically degenerate directions [oblique rolls, (OR)], while above the cutoff frequency f_c the fine rolls of the "dielectric" electroconvection pattern takes over. In the following we will focus our attention on the "conductive" regime only. The theoretical description of electroconvection based on the Carr-Helfrich mechanism has been well established during the past decades and is often referred to as the standard model [1,15]. According to that, V_c and the wave vector $\vec{q}_c$ at onset can be obtained from a linear stability analysis of the equations of nematodynamics.

Increasing the applied voltage V above V_c [i.e., if the dimensionless control parameter $\varepsilon = (V^2 - V_c^2)/V_c^2 > 0$] the morphology of the pattern may change and secondary EC instabilities may appear. This regime is usually described by the very powerful tools of the weakly nonlinear analysis (WNA) leading to Ginzburg-Landau equations (GLE) [1,15]. An important example of the secondary EC instabilities is the transition to the *abnormal roll* (AR) pattern which is characterized by an excursion of the director in the xy plane with respect to its initial direction while keeping the roll direction unaltered [16,17]. As the surfaces exert no azimuthal restoring torques on the director in a homeotropic cell, ARs can be easily observed experimentally by the net rotation of the optical axis of the slab [12–14,18]. The exploration of abnormal rolls demonstrated a previously unregarded symmetry breaking of the system and pointed out the necessity of a coupling between the pattern amplitude A and the azimuthal angle φ of the director [19,20]. With this extension of the GLE the NR-AR transition appears as a supercritical pitchfork bifurcation with a twofold degeneracy of the azimuthal rotation which has been proved experimentally recently both for planar orientation [21,22] and for homeotropic cells at a fixed small magnetic field [12,14].

In previous experimental studies on electroconvection in homeotropic cells a magnetic field was mainly used to stabilize the pattern only (to prevent from spatiotemporal chaos). The H dependence of EC patterns in MBBA (methoxybenzilidene butilaniline) has been tested only recently with emphasis on pattern dynamics and on novel scenarios at high magnetic fields [8,10]. In the present paper we mainly concentrate on the influence of a small magnetic field. In the following we first describe our experimental setup and evaluation method. We continue with our results on the Fréedericksz state, and on the characteristics of the EC patterns at onset. Then we discuss the magnetic field dependence of the NR-AR transition and conclude with a comparison to theoretical predictions.

II. EXPERIMENT

The H dependence of the EC transitions was investigated in homeotropic samples of the nematic mixture Phase 5A (Merck). The substance was selected due to its chemical stability, wide frequency range for NR, and known material parameters [23]. The thickness d of the sandwich cells,

26 μm and 46 μm, respectively, was determined by a spectrophotometer before filling. The electric field was applied to the transparent indium-tin-oxide electrodes of about 1.5 cm $\times$1.5 cm surface. Owing to its dissolved surfactant content, Phase 5A tends to align homeotropically on thoroughly cleaned glass surfaces, so no additional surface treatment was necessary to obtain a good alignment. The temperature of the cell was kept constant in a thermostatted chamber at $T=30.0\pm0.1\,°C$ by circulating water. The chamber was placed into an electromagnet with the magnetic field parallel to the cell surfaces (along $\vec{x}$). Varying the current the magnetic field could be controlled in the range $((1/\mu_0)26$ mT $<H<(1/\mu_0)1$ T) and was monitored by a Hall sensor. The cell was driven by a sinusoidal voltage from a PC controlled function generator through a high voltage amplifier, the actual ac voltage on the cell was measured by a true rms voltmeter.

The electroconvection patterns were observed by a Questar long range microscope from a working distance of about 30 cm while the cell was illuminated by polarized white light. The blue part of the visible spectrum was cut out with a yellow filter in order to avoid local heating of the cell due to the absorbtion of the liquid crystal. The microscope was equipped with a charge-coupled device video camera whose output was connected to a frame grabber card in a PC. This allowed on-line manipulations and recording of the live or digitally processed images with a resolution of 512×512 square pixels and 256 gray levels. Moreover, the camera could be used to measure the spatial distribution of the light intensity in the pattern. Both the polarizer and the analyzer in the light path could be rotated by stepper motors in steps of $1.8°$ (200 steps per revolution) either independently or synchronously. Stepping was synchronized to the video recording rate (25 frames/s) allowing one step of rotation for each video frame, thus a full revolution of the polars took 8 s.

The direction of the local director as well as the contrast of the pattern were determined by digital image processing when rotating the polars. For this purpose a single row of the image ($y=$const) was selected and the same row taken at subsequent angular positions α of the polarizer was copied into the subsequent rows of a new image called the $x-\alpha$ image. The $x-\alpha$ images allowed a direct visualization of both the spatial and α dependence of the light intensity.

In the classical shadowgraph arrangement a single polarizer is used [24]. The pattern is visible in extraordinary illumination only, thus the $\delta I=I_{max}-I_{min}$ modulation of the light intensity (I_{max} is the maximum, I_{min} the minimum intensity within a roll) varies upon rotation of the polarizer according to

$$\delta I(\alpha)=\Delta I_0 \cos^2(\alpha-\varphi). \tag{1}$$

The contrast defined as

$$A=\frac{I_{max}-I_{min}}{I_{max}+I_{min}} \tag{2}$$

can then be used as a measure of the pattern amplitude.
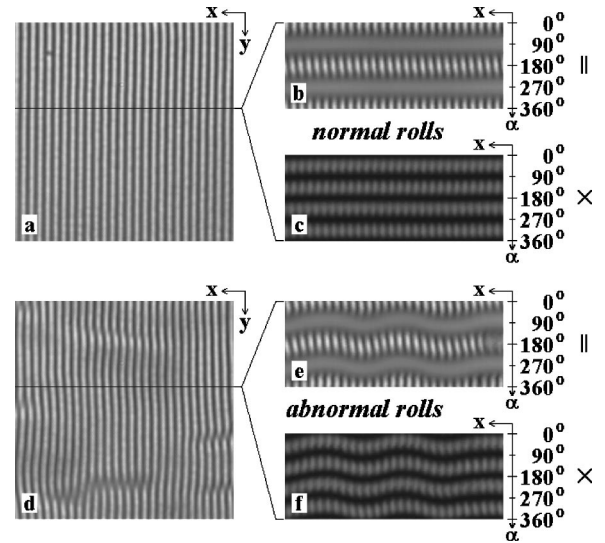
FIG. 1. Electroconvection patterns in a homeotropic cell of Phase 5A. $d=26$ μm, $f=1000$ Hz. Normal rolls: Snapshot with parallel polars (a), $x-\alpha$ image with parallel (b) and with crossed (c) polars. Abnormal rolls: Snapshot with parallel polars (d), $x-\alpha$ image with parallel (e) and with crossed (f) polars. The size of the snapshot images is 768 μm$\times$783 μm.

In case of parallel polars the actual $\delta I(\alpha)$ dependence becomes more complicated due to the influence of the birefringence of the sample, however, it still holds that the pattern should disappear in the $x-\alpha$ image twice per revolution (at the ordinary illumination) as shown in Figs. 1(b) and 1(e). Hence the contrast defined above approximates well the pattern amplitude as long as the voltage applied is near the threshold.

In the case of crossed polars, the intensity I of the image varies as

$$I(\alpha)=I_0 \sin^2 2(\alpha-\varphi), \tag{3}$$

thus the $x-\alpha$ image should contain four extinction lines in each full revolution (two for the ordinary and another two for the extraordinary illumination). Here I_0 depends both on the intensity of the incoming light and on the birefringence of the nematic slab. The extinction lines must be straight as long as the azimuthal angle φ of the director is constant, but become modulated if φ has a spatial dependence. Figures 1(c) and 1(f) show examples for NR and AR, respectively. For the quantitative analysis of the $x-\alpha$ images the intensity modulation due to the pattern is smoothed out by averaging over the roll wavelength around a fixed x, then the α dependence of this averaged intensity is fitted to Eq. (3) to obtain the local azimuthal angle $\varphi(x)$ of the director. The minimum and maximum of $\varphi(x)$ are regarded as the measured values of φ_- and φ_+ respectively (see [12]).

III. THE FRÉEDERICKSZ STATE

Upon application of an ac voltage the sample first undergoes an electric bend Fréedericksz transition. The threshold voltage $V_F(H)$ decreases with the magnetic field following
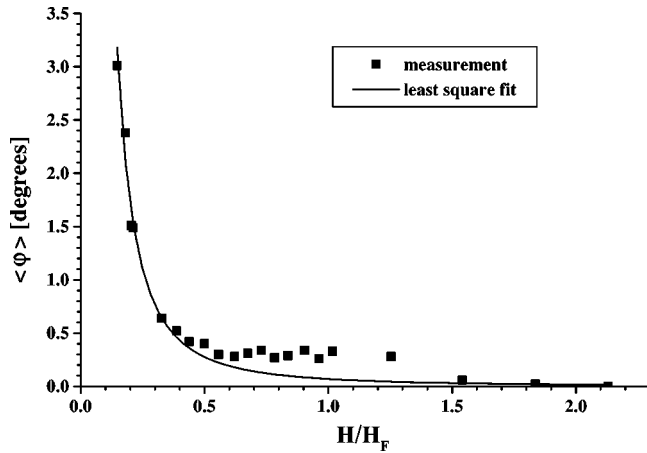
FIG. 2. Magnetic field dependence of the azimuthal angle of the director in the Fréedericksz state. $\langle\rangle$ denotes averaging over x. $d = 26$ μm, $H_F = (1/\mu_0)285$ mT is the magnetic Fréedericksz threshold. The solid line represents a least squares fit to $\varphi(x) \propto H^{-2}$.

the $V_F(H) = V_{F0}\sqrt{1 - H^2/H_F^2}$ dependence calculated from the continuum theory of nematic liquid crystals [25,26] (see the solid line with stars in Fig. 5). Here V_{F0} is the threshold voltage in the absence of a magnetic field, while H_F is the magnetic Fréedericksz threshold at $V = 0$. $V_F(H)$ is independent of the frequency in the studied range as expected.

The ideal homeotropic situation is azimuthally degenerate, thus above the Fréedericksz transition $[V > V_F(H)]$ the director should tilt toward the direction of the magnetic field for any nonzero H. Experimentally some slight spatial variation of the azimuthal angle $\varphi(x)$ was detected, which scales with H as shown in Fig 2. This indicates the presence of a local azimuthal preference in the alignment, similar to that reported previously [27] in other substances. For such conditions a simple calculation yields, for not too low fields, $\varphi(x) \propto H^{-2}$ (solid line in Fig. 2), which seems to be fulfilled upto $H_F/3$, i.e., where φ exceeds the limit of the error. The deviation from the ideal alignment there was, however, even so small that it did not affect the studied phenomena.

IV. THE ELECTROCONVECTION THRESHOLD AND THE LIFSHITZ POINT

Electroconvection sets in at a threshold voltage V_c exceeding V_F. The patterns observed in the frequency range of $f = 150$–1500 Hz are characteristic of the conductive regime (f_c is well above 2 kHz). Below 150 Hz, however, a stationary roll pattern could not develop at V_c as it was overcome either by localized turbulent patches traveling through the sample or by an intermittent behavior. Figure 3 shows a typical example of the traveling paw like structures localized to regions with a diameter of about $6\lambda_c$-$8\lambda_c$. Their moving front resembles a dendritic growth [28], and is characterized by a fierce, chaotic convection leaving behind weakening traces of the roll pattern. In another scenario a similar front runs through the sample resulting in a transition from the developing weak roll pattern to a turbulent convection. This turbulent state decays spontaneously, partially recovering ho-
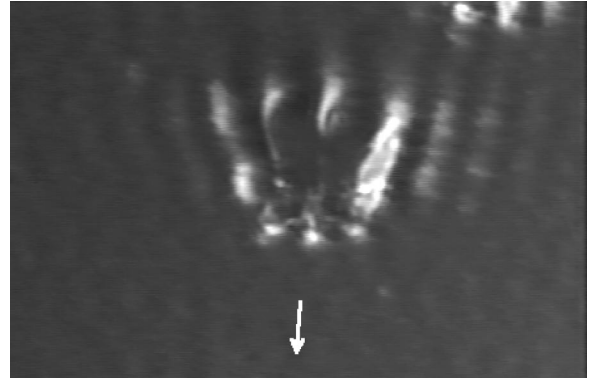
FIG. 3. Localized pawlike traveling electroconvection pattern in a homeotropic Phase 5A. The arrow indicates the direction of motion. $d = 26$ μm, $f = 100$ Hz.

mogeneous regions where EC can set in again. This process occurs repeatedly on the minute scale leading to oscillations between the two kinds of patterns at a constant voltage.

V_c showed the typical monotonic increase with the frequency for any H as shown in Fig. 4. The theoretical curve (solid line) calculated numerically for $H = 0.32 H_F$ is presented too. The magnetic field dependence of V_c showed pronounced differences in various frequency ranges. At low ($f < f_H \approx 650$ Hz) frequencies V_c first decreases with H exhibiting a pronounced minimum, while it increases monotonically at high ($f > f_H$) frequencies. The depth of the minimum as well as the magnetic field belonging to it are increasing with decreasing frequency. For a high magnetic field V_c always increases with H. The slope, however, starts to decrease at a frequency $f \approx 850$ Hz$> f_H$. This behavior is clearly demonstrated in Fig. 5 showing, in a wide H range, the variation of the thresholds $V_c(H)$ scaled by their value V_{c0} at the lowest field used ($H = 0.249 H_F$) in order to compensate for the strong frequency dependence of V_c. Such a minimum in $V_c(H)$ has neither been reported experimentally nor predicted theoretically to our knowledge yet (recent data
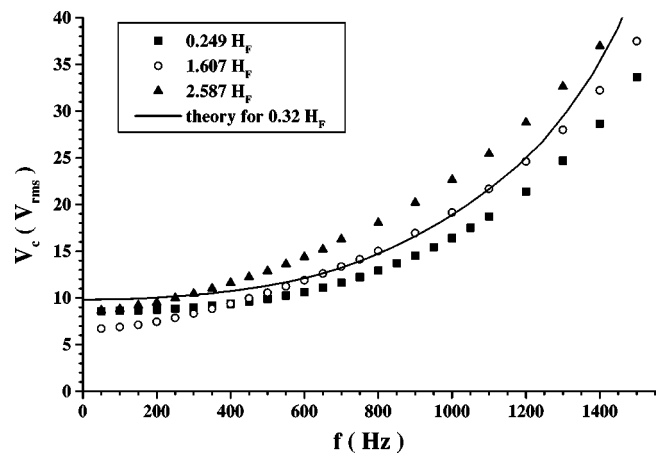
FIG. 4. Frequency dependence of the electroconvection threshold voltage at various magnetic fields. $d = 46$ μm, $H_F = (1/\mu_0)170$ mT. The solid line corresponds to the theoretical curve obtained numerically for $H = 0.32 H_F$.
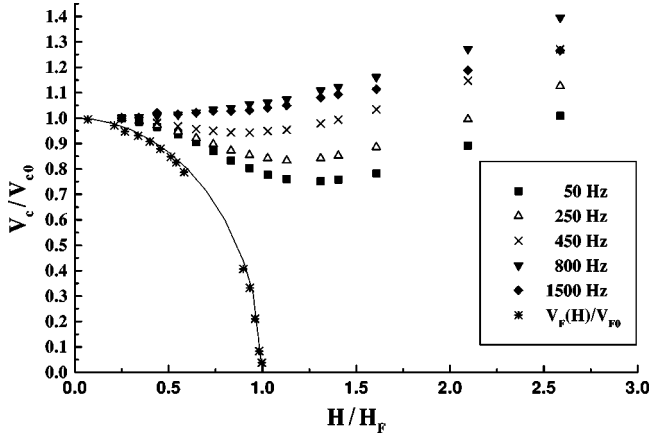
FIG. 5. Magnetic field dependence of the electroconvection threshold voltage at various frequencies. $d=46$ μm. The solid line corresponds to the theoretically expected H dependence of the Fréedericksz threshold voltage; stars are the measured values.

for homeotropic MBBA exhibit monotonic increase with H, though mainly for higher fields [10]).

The patterns developing at the onset of the electroconvection are either oblique (OR) or normal rolls (NR) depending on the frequency. They are characterized by two parameters, the wavelength λ_c and the tilt angle β of the rolls ($\beta=0$ for NR), which were obtained by computing the two-dimensional Fourier transforms of the recorded images. λ_c decreases with increasing the magnetic field, its variation with H diminishes for higher frequencies. λ_c decreases monotonically also with f at $H\approx0$, however, this fails at high fields when $\lambda_c(H)$ forms a maximum in the range 200 Hz $<f<500$ Hz as shown in Fig. 6.

Figure 7 exhibits the frequency dependence of the roll angles of the EC pattern. Remarkably, at a small magnetic field ($H=0.25H_F$), one finds $\beta\approx0$ not only for $f>f_L$ ≈850 Hz but for $f<f_{L2}\approx250$ Hz as well, i.e., the system possesses two Lifshitz points. Oblique rolls appear only for
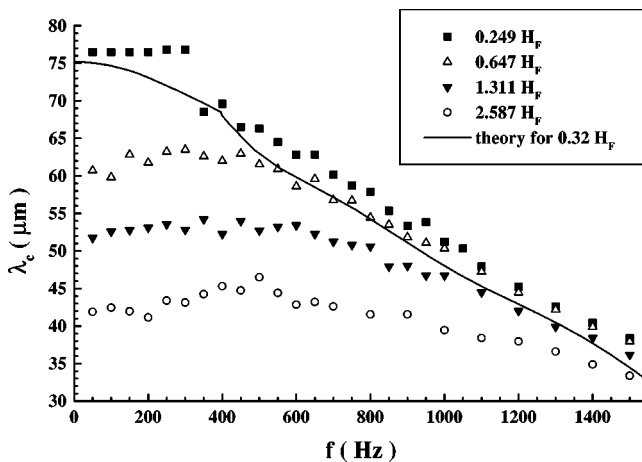
FIG. 6. Frequency dependence of the wavelength of the electroconvection patterns at various magnetic fields. $d=46$ μm. The solid line corresponds to the theoretical curve obtained numerically for $H=0.32H_F$.
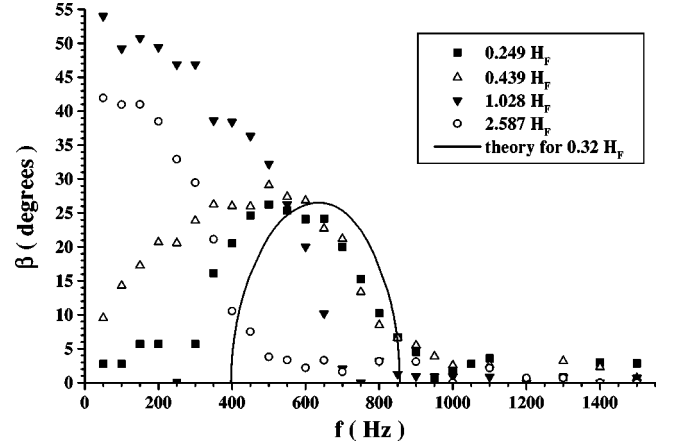
FIG. 7. Frequency dependence of the roll angle in a homeotropic cell of Phase 5A at various magnetic fields. $d=46$ μm. The solid line corresponds to the theoretical curve obtained numerically for $H=0.32H_F$.

$f_{L2}<f<f_L$ with a maximum of the obliqueness in between. This behavior is quite unusual, because if oblique rolls appear at all, they were observed always at low frequencies (in planar samples as well as in homeotropic MBBA [7,10]). Though we have already reported recently about measurements in homeotropic Phase 5A indicating the existence of a second Lifshitz point in agreement with numerical calculations [12–14], the low frequency "reentrant" normal rolls at $f<f_{L2}$ have also been detected now, as is demonstrated by the snapshots in Fig. 8.

Increasing the magnetic field f_{L2} is first shifted below the lowest measuring frequency ($f=50$ Hz) though still keeping the nonmonotonic behavior of $\beta(f)$, while for higher H the usual monotonic dependence is obtained. The maximal roll angle first increases with the field reaching a maximum of about $55°$ at moderate H values, and decreases for high fields. This correlates with the nearly linear decrease of the upper Lifshitz point f_L as shown in Fig. 9.

V. THE NR-AR TRANSITION

The ε dependence of the azimuthal angle $\varphi_\pm$ of the director has been obtained from the WNA in the form [12]

$$\varphi_\pm = \begin{cases} \pm\Phi\sqrt{\varepsilon-\varepsilon_{AR}} & (\varepsilon>\varepsilon_{AR}) \\ 0 & (\varepsilon<\varepsilon_{AR}), \end{cases} \qquad (4)$$
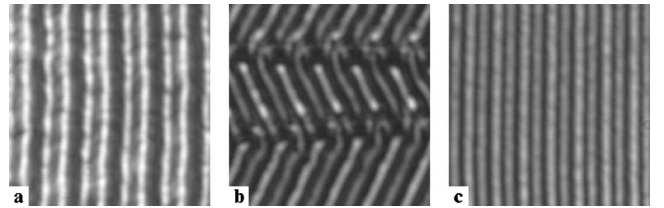
FIG. 8. Snapshots of the electroconvection patterns in a homeotropic Phase 5A slightly above onset at various frequencies. (a) reentrant normal rolls at $f<f_{L2}$; (b) oblique rolls at $f_{L2}<f<f_L$; (c) normal rolls at $f>f_L$. The size of the images is 384 μm $\times391$ μm, $d=46$ μm, $H=42.4$ mT$=0.249H_F$.
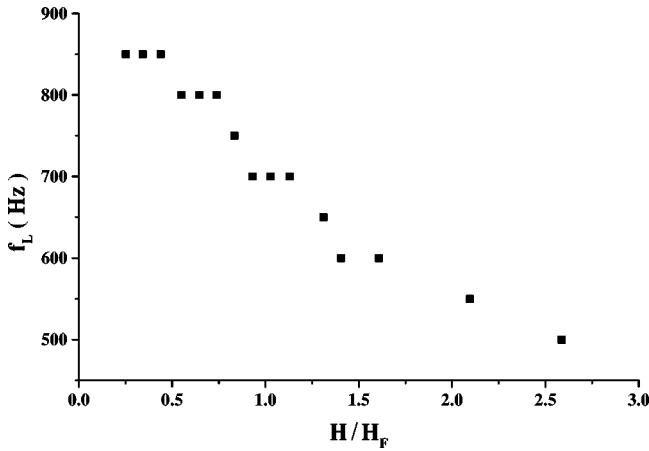
FIG. 9. Magnetic field dependence of the Lifshitz point f_L. $d=46$ μm.

where $\varepsilon_{AR}=(V_{AR}^2-V_c^2)/V_c^2$, V_{AR} is the threshold for ARs and Φ provides the magnitude of the opening angle of the pitchfork.

In the limit of $H\rightarrow 0$ ε_{AR} is also small and can be calculated together with Φ yielding

$$\varepsilon_{AR}=2gH^2/(H_F^2|\Gamma|q_c^2) \qquad (5)$$

and

$$\Phi=(\xi_{yy}q_c)^{-1}. \qquad (6)$$

Here q_c is the wave number at onset, ξ_{yy} is the correlation length of the pattern, g and Γ are parameters of the extended GLE. It can be seen that ε_{AR} is tunable by the magnetic field ($\varepsilon_{AR}\propto H^2$ for small H).

In order to study the H dependence of the NR-AR transition, the applied voltage was increased in small steps ($\Delta\varepsilon\approx 0.001-0.01$ depending on H) in a wide range of magnetic fields ($0.1H_F<H<2H_F$) and the azimuthal angles $\varphi_\pm$ as well as the contrast (the pattern amplitude) were measured using the rotating polarizers technique (see Fig. 1).

Figure 10 shows the typical ε dependence of $\varphi_\pm$ for a small and a high H, clearly demonstrating the pitchfork bifurcation, characteristic of the NR-AR transition. Fitting data with Eq. (4), the threshold ε_{AR} as well as the opening angle Φ could be obtained.

Figure 11 exhibits the NR-AR transition (defined as ε_{AR}) as a function of the magnetic field. The magnetic field dependence of Φ is presented in Fig. 12. The solid curves in both figures correspond to the theoretical predictions discussed in the following section.

We want to mention that the above results have been obtained on samples exhibiting a continuous transition (forward bifurcation) at the onset of electroconvection. The ionically doped Phase 5A, however, can be shifted into a parameter range (enhanced conductivity via ageing) where the transition to EC occurs through a backward bifurcation with a pronounced jump in the pattern amplitude at onset.

Backward transitions in electroconvection are not unprecedented, they have been reported to exist under appropriate
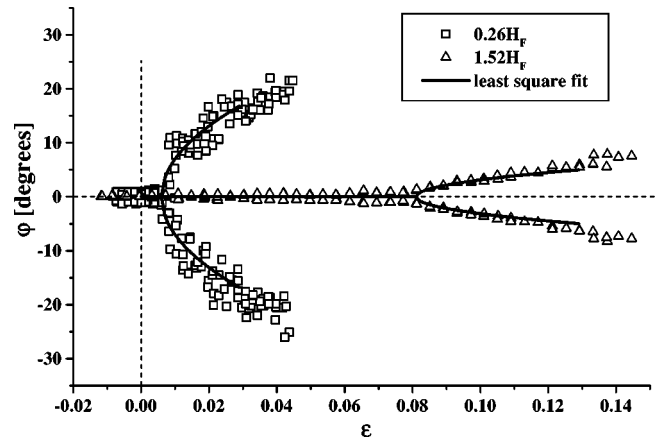
FIG. 10. ε dependence of the azimuthal angle of the director at $H=0.26H_F$ (open squares) and at $H=1.52H_F$ (open triangles). The solid curves correspond to fits to Eq. (4) with $\varepsilon_{AR}=0.006$, $\Phi=110°$ and $\varepsilon_{AR}=0.081$, $\Phi=22°$, respectively. $d=26$ μm, $f=1000$ Hz.

conditions for various substances (MBBA [29], I52 [30], Phase 5 [31]). In some previously reported cases [31] the jump in the amplitude occurred above the onset as a consequence of a transition from traveling waves into stationary rolls, thus the pattern characteristics have also changed simultaneously. This is not the case here, the wavevector and the dynamics of the pattern remain unaltered. The detailed study of the phenomenon is in progress.

In agreement with earlier measurements [13,14] it was also found that in AR domains the distribution of the director is not homogeneous, it is rather characterized by a continuous spatial modulation of the azimuthal angle [see Figs. 1(e,f)]. At low $\varepsilon-\varepsilon_{AR}$ values $|\varphi|$ is small and the AR domains are large and patchy. Increasing ε at medium $H\approx 1/3H_F$ fields the AR domains become elongated along the convection rolls and form almost periodic structures containing typically 4–6 rolls. These AR domains thus represent an example of patterns with a characteristic wavelength much
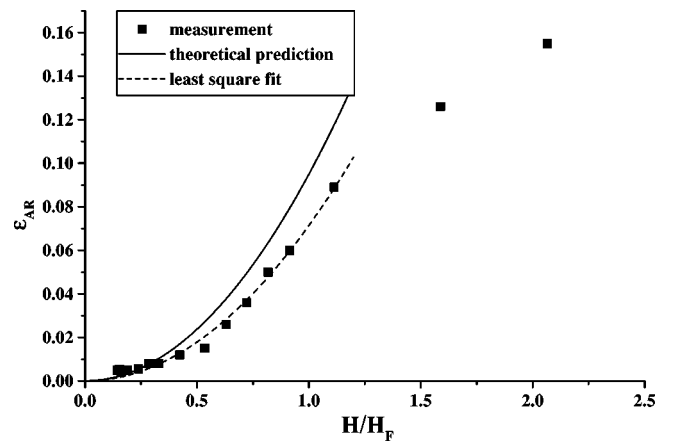
FIG. 11. Magnetic field dependence of the threshold ε_{AR} of the NR-AR transition. $d=46$ μm, $f=1000$ Hz. The solid line corresponds to the theoretical prediction, the dotted one represents a least squares fit.
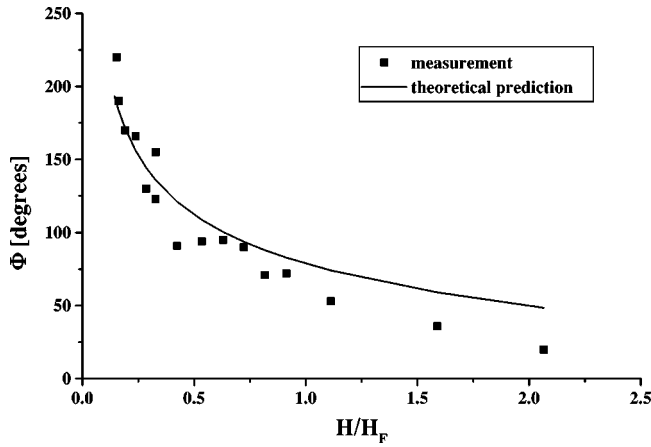
FIG. 12. Magnetic field dependence of the opening angle Φ characterizing the NR-AR transition. $d=46$ μm, $f=1000$ Hz. The solid line corresponds to the theoretical prediction [Eq. (6)].

exceeding the sample thickness. It should be mentioned that at low magnetic fields this AR domain structure develops into a defect mediated chevron pattern [32,33] if ε is increased appropriately [14].

At large magnetic fields ($H \gtrsim H_F$), however, the characteristics of the AR domains change. The spatial variation of φ becomes restricted to a narrow transition area—a domain wall—where φ changes its sign, while φ will be constant within the domains. That is clearly seen both from the snapshots and the $x-\alpha$ images in Fig. 13(a–d) where the domain walls are parallel to the rolls. Within a single AR domain the roll pattern can either be homogeneous [Fig. 13(a) left] or may contain long defects running across the rolls. These defects are characterized by a phase jump of about π which is clearly seen in the right hand side of Fig. 13(a) and result additionally in a zigzag modulation of the roll directions.
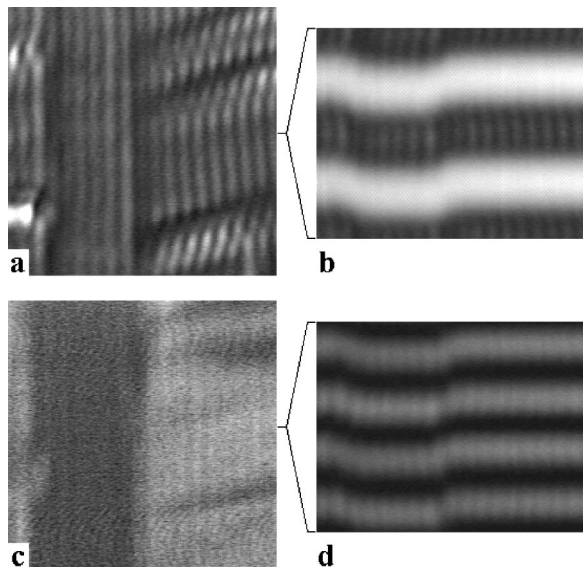
FIG. 13. Abnormal roll domains at $H=1.05H_F$. Snapshot (a) and $x-\alpha$ image (b) at parallel polars, snapshot (c) and $x-\alpha$ image (d) at crossed polars. $d=26$ μm, $f=1100$ Hz, the size of snapshot images is 384 $\mu \times 391$ μm.
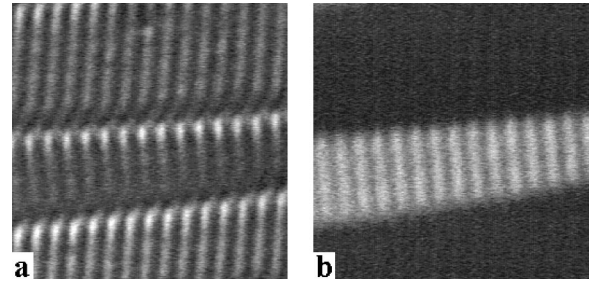
FIG. 14. Abnormal roll domains at $H=1.45H_F$. Snapshot at parallel (a) and at crossed (b) polars. $d=26$ μm, $f=1000$ Hz, the size of snapshot images is 384 $\mu \times 391$ μm.

These defects may be examples of the phase jump lines described theoretically recently [34]. Changing the frequency and/or H, however, one can find domain walls running almost normal to the rolls [Figs. 14(a,b)] with an even more pronounced zigzag roll structure, similar to that in the oblique roll regime. This phenomenon is subjected to further investigation.

VI. CONCLUSIONS

In order to compare our data with the theoretical predictions of the linear analysis the numerically calculated frequency dependences of V_c, λ_c and β are also plotted in Figs. 4, 6, and 7, respectively. These curves were obtained [12] for $H=0.32H_F$ using the measured set of material parameters of Phase 5 [23] keeping the electrical conductivity $\sigma_\perp$ as the only fit parameter that was adjusted to obtain the best match for all curves. The agreement for small magnetic fields is fairly good, indicating that the standard model of EC can account even for the existence of two Lifshitz points.

It should be mentioned here that the Lifshitz point(s) are very sensitive to some material constants. Similar calculations using the typical set of material parameters of MBBA did not lead to the appearance of a second Lifshitz point [35]. This also seems to match experimental findings as MBBA either possessed a monotonic $\beta(f)$ dependence [7], or exhibited just a faint tendency for a maximum [10].

Unfortunately no detailed theoretical predictions or numerical calculations are currently available for the magnetic field dependence of the pattern characteristics. One can notice, however, that the anomalies in the threshold and/or the roll angles of the EC pattern occur in that frequency (and magnetic field) range where V_c is just slightly above V_F. The director profile in the Fréedericksz state, which the electroconvection pattern is superposed on, depends on V_c/V_F. For small values of V_c/V_F the Fréedericksz deformation is not very pronounced, i.e., the tilt angle (with respect to $\vec{z}$) of the director at midplane is still small, the director is far from planar. However, a planar director is a better starting point for the Carr-Helfrich EC mechanism to work than a (homogeneously) tilted one. (Actually the EC threshold voltage of a planar cell is lower than that of a homeotropic one.) As the applied magnetic field pushes the director further toward $\vec{x}$, the EC threshold can go down. At higher frequencies and/or at high magnetic fields, however, V_c/V_F becomes large so

the director is nearly planar already at the threshold. An (additional) magnetic field still pushes the director toward $\vec{x}$, but now it has rather the effect of inhibiting EC (preventing from the periodic tilt deformation required) therefore V_c goes up. The observed minimum in $V_C(H)$ thus seems to be intuitively understandable.

Similar reasoning leads to the expectation of a backward bifurcation when V_c is just slightly above V_F. When the Fréedericksz deformation is small, finite-amplitude convection may lead the director into a more favorable average orientation, requiring a smaller driving force. This behavior is known from EC in planarly aligned systems with an additional magnetic field in the z direction well above the Fréedericksz value [36]. Then one also has in the nonconvecting state a director that is nearly parallel to $\vec{z}$. One finds localized states that can take the character of moving dendrites [28].

According to Eq. (5) the theory predicts a quadratic dependence of ε_{AR} on H with a calculated coefficient of 0.095 (see the solid line in Fig. 11). This decribes the experimental data very well upto rather high ($H \approx H_F$) magnetic fields. A least square fit of $\varepsilon_{AR} \propto H$ to the experimental points (depicted by dotted line in the same figure) yields the rather close value 0.071 for the same coefficient. At present, there are no predictions for the behavior at high ($H > H_F$) fields.

Equation (6) does not explicitly show a H dependence, nevertheless, it incorporates one implicitly. The measurements have been carried out at a constant physical frequency f, however, due to the magnetic field induced shift of the Lifshitz point (see Fig. 9) the same f corresponds to increasing values on the relative frequency scale of f/f_L for increasing H. It has already been shown [12] that Φ depends strongly on f/f_L, diverging at the codimension 2 point [21,22] (slightly above the Lifshitz point). The solid line in Fig. 12, calculated by taking into account this variation of the relative frequencies, provides excellent agreement with the experimental data. The slight deviation for $H > H_F$ is plausible as Eqs. (5) and (6) strictly hold for small magnetic fields only.

[1] L. Kramer and W. Pesch, in *Pattern Formation in Liquid Crystals*, edited by Á. Buka and L. Kramer (Springer-Verlag, New York, 1996).

[2] A. Hertrich, W. Decker, W. Pesch, and L. Kramer, J. Phys. II **2**, 1915 (1992).

[3] S. Kai, K. Hayashi, and Y. Hidaka, J. Phys. Chem. **100**, 19 007 (1996).

[4] H. Richter, Á. Buka, and I. Rehberg, Phys. Rev. E **51**, 5886 (1995).

[5] Y. Hidaka, J.-H. Huh, K. Hayashi, M.I. Tribelsky, and S. Kai, J. Phys. Soc. Jpn. **66**, 3329 (1997).

[6] Y. Hidaka, J.-H. Huh, K. Hayashi, S. Kai, and M.I. Tribelsky, Phys. Rev. E **56**, R6256 (1997).

[7] P. Tóth, Á. Buka, J. Peinke, and L. Kramer, Phys. Rev. E **58**, 1983 (1998).

[8] J.-H. Huh, Y. Hidaka, and S. Kai, J. Phys. Soc. Jpn. **67**, 1948 (1998).

[9] H. Richter, N. Klöpper, A. Hertrich, and Á. Buka, Europhys. Lett. **30**, 37 (1995).

[10] J.-H. Huh, Y. Hidaka, and S. Kai, J. Phys. Soc. Jpn. **68**, 1567 (1999).

[11] J.-H. Huh, Y. Hidaka, and S. Kai, Mol. Cryst. Liq. Cryst. Sci. Technol., Sect. A **328**, 497 (1999).

[12] A.G. Rossberg, N. Éber, Á. Buka, and L. Kramer, Phys. Rev. E **61**, R25 (2000).

[13] A.G. Rossberg, N. Éber, Á. Buka, and L. Kramer, Mol. Cryst. Liq. Cryst. Sci. Technol., Sect. A **351**, 161 (2000).

[14] Á. Buka, P. Tóth, N. Éber, and L. Kramer, Phys. Rep. **337**, 157 (2000).

[15] E. Bodenschatz, W. Zimmermann, and L. Kramer, J. Phys. (France) **49**, 1875 (1988).

[16] H. Richter, Á. Buka, and I. Rehberg, Mol. Cryst. Liq. Cryst. Sci. Technol., Sect. A **251**, 181 (1994).

[17] H. Richter, Á. Buka, and I. Rehberg, in *Spatio-Temporal Patterns*, edited by P.E. Cladis and P. Palffy-Muhoray (Addison-Wesley, Reading, MA, 1995), p. 343.

[18] J.-H. Huh, Y. Hidaka, and S. Kai, Phys. Rev. E **58**, 7355 (1998).

[19] A.G. Rossberg, A. Hertrich, L. Kramer, and W. Pesch, Phys. Rev. Lett. **76**, 4729 (1996).

[20] A.G. Rossberg and L. Kramer, Phys. Scr., T **T67**, 121 (1996).

[21] E. Plaut, W. Decker, A.G. Rossberg, L. Kramer, W. Pesch, A. Belaidi, and R. Ribotta, Phys. Rev. Lett. **79**, 2367 (1997).

[22] S. Rudroff, H. Zhao, L. Kramer, and I. Rehberg, Phys. Rev. Lett. **81**, 4144 (1998).

[23] M. Treiber, N. Éber, Á. Buka, and L. Kramer, J. Phys. II **7**, 649 (1997).

[24] S. Rasenat, G. Hartung, B.L. Winkler, and I. Rehberg, Exp. Fluids **7**, 412 (1989).

[25] P.G. deGennes, *The Physics of Liquid Crystals* (Clarendon Press, Oxford, 1974).

[26] S. Chandrasekhar, *Liquid Crystals* (Cambridge University Press, Cambridge, 1992).

[27] I. Jánossy and A. Jákli, Mol. Cryst. Liq. Cryst. Sci. Technol., Sect. A **251**, 255 (1994).

[28] J.T. Gleeson, Nature (London) **385**, 511 (1997).

[29] I. Rehberg, S. Rasenat, M. de la Torre Juarez, W. Schöpf, F. Hörner, G. Ahlers, and H.R. Brand, Phys. Rev. Lett. **67**, 596 (1991).

[30] M. Dennin, Ph.D. thesis, University of Santa Barbara, 1995 (unpublished).

[31] M. de la Torre Juarez and I. Rehberg, Phys. Rev. A **42**, 2096 (1990).

[32] A.G. Rossberg and L. Kramer, Physica D **115**, 19 (1998).

[33] J.-H. Huh, Y. Hidaka, A.G. Rossberg, and S. Kai, Phys. Rev. E **61**, 2769 (2000).

[34] H. Zhao, *Secondary Instabilities and Complex Patterns in Anisotropic Convection* (Dissertations Verlag NG Kopierladen, München, 2000).

[35] A. Hertrich, Ph.D. thesis, University of Bayreuth, 1995 (unpublished).

[36] A. Hertrich, W. Pesch, and J.T. Gleeson, Europhys. Lett. **34**, 417 (1996).